

Katherine Acton¹

Department of Mechanical Engineering,
University of St. Thomas,
St. Paul, MN 55105
e-mail: kacton@stthomas.edu

Connor Sherod

Department of Mechanical Engineering,
University of St. Thomas,
St. Paul, MN 55105
e-mail: sher7302@stthomas.edu

Bahador Bahmani

Department of Mechanical, Aerospace, and
Biomedical Engineering,
University of Tennessee Knoxville (UTK)/
Space Institute (UTSI),
Tullahoma, TN 37388
e-mail: bbahmani@vols.utk.edu

Reza Abedi

Department of Mechanical, Aerospace, and
Biomedical Engineering,
University of Tennessee Knoxville (UTK)/
Space Institute (UTSI),
Tullahoma, TN 37388
e-mail: rabedi@utk.edu

Effect of Volume Element Geometry on Convergence to a Representative Volume

To accurately simulate fracture, it is necessary to account for small-scale randomness in the properties of a material. Apparent properties of statistical volume element (SVE) can be characterized below the scale of a representative volume element (RVE). Apparent properties cannot be defined uniquely for an SVE, in the manner that unique effective properties can be defined for an RVE. Both constitutive behavior and material strength properties in SVE must be statistically characterized. The geometrical partitioning method can be critically important in affecting the probability distributions of mesoscale material property parameters. Here, a Voronoi tessellation-based partitioning scheme is applied to generate SVE. Resulting material property distributions are compared with those from SVE generated by square partitioning. The proportional limit stress of the SVE is used to approximate SVE strength. Superposition of elastic results is used to obtain failure strength distributions from boundary conditions at variable angles of loading. [DOI: 10.1115/1.4043753]

1 Introduction

When a material is modeled as homogeneous in a fracture simulation, the simulation will not accurately capture the small-scale randomness inherent in crack propagation due to microstructural heterogeneity. However, direct simulation of material flaws, defects, pores, or inclusions may be infeasible due to computational expense, and/or material characterization may not be available in sufficient detail. Therefore, probabilistic continuum models are needed that accurately characterize both material properties and variability in material properties at a relatively small scale. Traditional representative volume element (RVE) approaches in modeling heterogeneous material provide a continuum approximation, but obscure local material variability. Statistical volume element (SVE) approaches provide a continuum approximation of material properties at a mesoscale, where d is the length scale of a typical microstructural feature (e.g., inclusion radius) and L is the macroscopic scale of the structure, and the size of the SVE and RVE (l_{SVE} and l_{RVE} , respectively) are ordered as follows:

$$d < l_{SVE} < l_{RVE} \ll L \quad (1)$$

A principal challenge with SVE approaches is the nonuniqueness of material properties obtained at a scale below the scale of an RVE. Extensive literature is devoted to the dependency of SVE apparent properties on the boundary conditions used to obtain the stress–strain relationship [1–6]. SVE can be used to generate statistical characterizations of random fields of material properties, which can be performed for use in stochastic simulation [7–10]. Often, analysis of the accuracy of SVE material properties is considered as a function of SVE size. Increasing the size of an SVE increases the accuracy of elastic results. However, whether a

phenomenological model such as Weibull model [11] is used [12,13], or strength is directly characterized by SVEs [14,15], the material inhomogeneity is lost at larger representation/averaging sizes. Moreover, strength properties tend to decrease as the size of an SVE increases, a phenomenon known as the size effect. To limit the size effect and maintain fracture strength inhomogeneities—which are particularly important for fragmentation studies [13,16]—unlike elastic results, it is thus preferred to limit the use of large scale SVE (and RVE) for strength predictions.

Statistical volume elements partition shape influences the determination of individual SVE properties, as well as statistics drawn from a population of SVE that partition an RVE. Partitioning a microstructure with inclusions into collections of Voronoi cells has been shown to provide an advantage over square partitioning [17,18]. Using Voronoi cell partitioning, inclusions do not intersect partition boundaries, avoiding the introduction of spurious stress concentrations. Based on this observation, previous work has focused on comparison of elastic material property statistics obtained by square and Voronoi partitioning. The current work extends previous results to focus on comparison of material strength properties obtained by square and Voronoi partitioning. In particular, the dependence of material strength on the angular direction of loading is investigated. The angular dependence of strength is important to statistically characterize, as it affects directionality of crack propagation in a fracture analysis.

2 Square and Voronoi Partitioning of Statistical Volume Elements

A typical square and Voronoi partitioning of an RVE is shown in Fig. 1. In this illustration, the side length of the SVE is ten times the length of the inclusion diameter. In general, a nondimensional parameter δ is defined to characterize SVE size, given as

$$\delta = l_{SVE}/l_{RVE} \quad (2)$$

¹Corresponding author.

Manuscript received February 18, 2019; final manuscript received May 3, 2019; published online June 5, 2019. Assoc. Editor: George Stefanou.

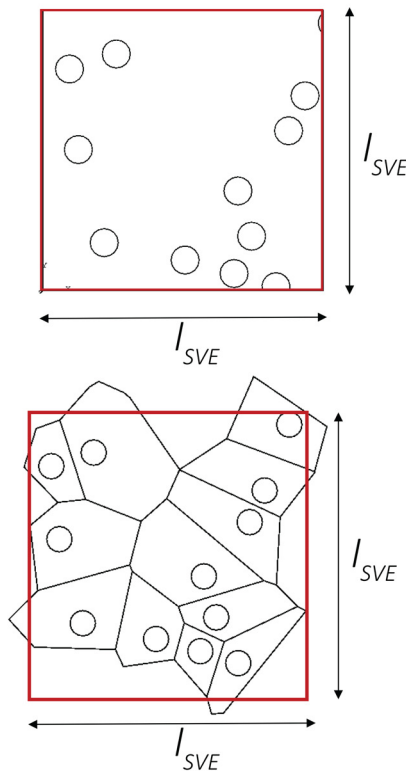
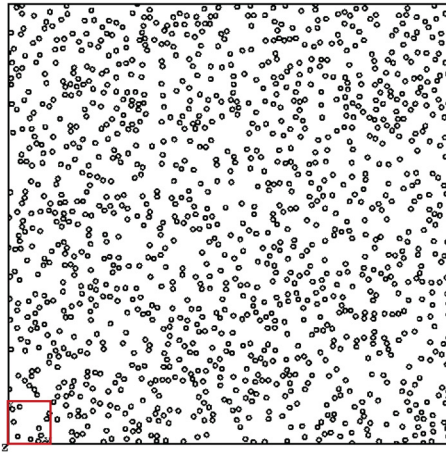


Fig. 1 Partitioning of RVE microstructure (top) into square and Voronoi SVE (middle and bottom figures, respectively) each with side length S

with variables as defined in Eq. (1). In this work, the side length of the square RVE is set to a unit value, and the inclusion diameter is $d = l_{RVE}/100$. To create SVE, the RVE side length is partitioned by powers of two to generate SVE with sizes $\delta = (1/4), (1/8)$, and $(1/16)$. This leads to populations sizes where $n = 16, 64$, and 256 , respectively.

Square partitioning is a straightforward method that ensures each SVE will be of uniform area, although partition boundaries often intersect inclusions, as shown in the figure. Voronoi partitioning is based on an underlying square partition of the RVE. In a given square region, if the centroid of a Voronoi cell lies within this region, the cell is assigned to the corresponding SVE. This leads to SVE with areas that have relatively high variation at small SVE sizes, and relatively low variation at large SVE sizes. As shown in the figure, the Voronoi cell partitioning approach does not allow inclusions to intersect partition boundaries. For more

details on the partitioning method used in this analysis, see Refs. [18] and [19].

3 Determination of Statistical Volume Elements Failure Strength

Material properties determined on an SVE are nonunique, and depend on applied boundary conditions and material properties of the matrix and inclusion. Both phases are assumed to be isotropic with Poisson's ratio of 0.3 and elastic moduli of 1 and 100 for the matrix and inclusion, respectively. In this work, a set of mixed uniform boundary conditions is applied, with displacement conditions in plane in two-dimensional (2D) elements under plane stress. Superposition is used to combine hydrostatic, pure, and simple shear boundary conditions (denoted H , P , and S) such that these results can be used to span the space of applied strains. This process and the method for determining failure strength as a function of load angle are briefly summarized here, and explained in more detail in Ref. [19].

The displacement condition is given as

$$\mathbf{u}|_{\partial\Omega} = \mathcal{E} \cdot \mathbf{x} \rightarrow \langle \varepsilon \rangle_{\Omega} = \mathcal{E} \quad (3)$$

where $\partial\Omega$ is the boundary of the body Ω , $\langle \varepsilon \rangle$ denotes average strain, and \mathcal{E} is a constant value.

Hydrostatic (H), pure shear (P), and simple shear (S) loading conditions are given by the three values of \mathcal{E} below, respectively,

$$\mathcal{E} = e^H \cdot \begin{bmatrix} 1 & 0 \\ 0 & 1 \end{bmatrix} \\ e^P \cdot \begin{bmatrix} 1 & 0 \\ 0 & -1 \end{bmatrix} \\ e^S \cdot \begin{bmatrix} 0 & 1 \\ 1 & 0 \end{bmatrix} \quad (4)$$

With a known uniform strain condition applied at the boundary of the SVE for each of the three principal loading directions, the average stress in the SVE is then calculated using finite element analysis. Using the prescribed strain/average stress relationship for H , P , and S strains, a stiffness matrix is calculated for each SVE.

The maximum stress at the matrix–inclusion boundary, in the direction normal to the inclusion, is also found for each SVE under H , P , and S applied loading. Results are superposed to generate results for normal and shear load applied from angles of 0–180 deg. A threshold value σ^{TH} is set such that when this value is exceeded at the matrix–inclusion interface, the material has reached an elastic limit signifying failure. Although this is not the ultimate fracture strength, for brittle and quasi-brittle materials, this threshold value is shown to be a close approximation for quasi-static [20] and low-rate dynamic loadings [21]. The same assumption is used in prior work for microcracked domains [16] and random composites [15,19].

The point at which the maximum matrix–inclusion boundary stress reaches the threshold value is calculated for two specific cases at each load angle θ . First, as shown in Fig. 2, the average normal SVE stress is fixed to have a unit value, with zero average shear stress. In this case, the strength value $\tilde{s}_n(\theta)$ is calculated, which can be multiplied by the maximum matrix inclusion interface stress to achieve the threshold value σ^{TH} . As shown in the figure, this corresponds to tensile strength of the SVE at angle θ . The $\pi/2$ angle shift between the angle of tensile strength and the average normal stress $\bar{\sigma}_{x'y'}$ is based on the convention with which tensile strength is often represented. Similarly, the shear strength $\tilde{s}_s(\theta)$ corresponds to a shear loading that would result in an average stress of the SVE with condition $\bar{\sigma}_{x'y'} = \bar{\sigma}_{y'y'} = 0$. The magnitude of the nonzero $\bar{\sigma}_{x'y'}$ is again chosen such that the fracture effective stress at one point on the interfaces between the

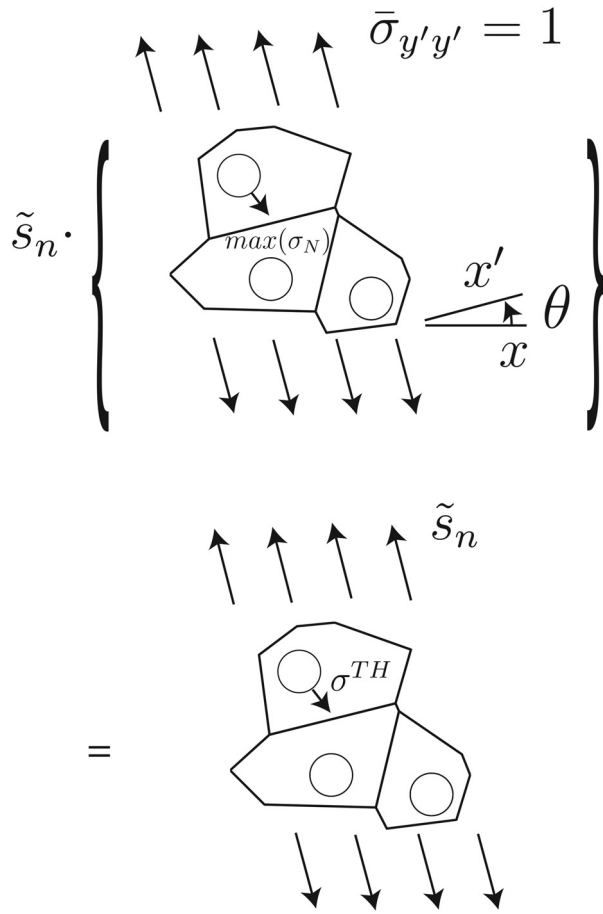


Fig. 2 Calculation of failure strength \tilde{s}_n . Failure occurs when the maximum stress on any inclusion boundary, in the direction normal to the inclusion, reaches a threshold value σ^{TH} [19].

inclusions and the matrix reaches σ^{TH} . More details on the calculation of $\tilde{s}_n(\theta)$ and $\tilde{s}_t(\theta)$ can be found in Ref. [19].

4 Determination of Statistical Volume Elements Maximum Wave Speed

To determine wave speeds, a solution must be obtained in the form

$$\mathbf{u} = \mathbf{U}f(\mathbf{x} \cdot \mathbf{n} - ct) \quad (5)$$

For a wave traveling in angle θ , the normal vector is $\mathbf{n} = [\cos \theta, \sin \theta]$. The space coordinate is $\mathbf{x} = [x_1, x_2]$ and time is given by t . The constant vector $\mathbf{U} = [U_1, U_2]$ represents the shape of displacement vector, c is the wave speed along the direction \mathbf{n} , and f is an arbitrary scalar function. By using the displacement–strain compatibility condition, constitutive equation between strain and stress, and the source free equation of motion for elastodynamic, the following eigenvalue problem is obtained:

$$\mathbf{Q}(\mathbf{C}, \mathbf{n})\mathbf{U} = \rho c^2 \mathbf{U} \quad (6)$$

where $\mathbf{Q}(\mathbf{C}, \mathbf{n})$ is the acoustic matrix. The relation between strain and stress is determined by the symmetric and positive definite 3×3 stiffness matrix, \mathbf{C} , in the Voigt notation. Since \mathbf{C} is symmetric and positive definite, so is the acoustic matrix and its eigenvalues, corresponding to ρc^2 , are positive. The components of the 2×2 acoustic matrix are given by

$$Q_{11} = C_{11}n_1^2 + 2C_{13}n_1n_2 + C_{33}n_2^2 \quad (7a)$$

$$Q_{12} = Q_{21} = C_{13}n_1^2 + (C_{12} + C_{33})n_1n_2 + C_{23}n_2^2 \quad (7b)$$

$$Q_{22} = C_{33}n_1^2 + 2C_{23}n_1n_2 + C_{22}n_2^2 \quad (7c)$$

for 2D elasticity, the eigenproblem (6) has two eigenvalues $\lambda \in \{\lambda_{\min}, \lambda_{\max}\}$. The corresponding wave speed for the eigenvalue λ is $c = \sqrt{\lambda/\rho}$. For an isotropic stiffness matrix, the maximum and minimum wave speeds correspond to longitudinal and shear wave speeds, respectively, which are equal for all directions θ .

For the SVEs, however, the homogenized stiffness matrix does not necessarily correspond to an isotropic material. Thus, the minimum and maximum wave speeds depend on $\mathbf{n} = [\cos \theta, \sin \theta]$. Accordingly, for each angle θ , the maximum nondimensional wave speed of an SVE is defined as

$$c_M(\theta) = \sqrt{\lambda_{\max}} \quad (8)$$

which is the maximum 2D wave speed of the SVE normalized by one-dimensional wave speed of the matrix (recalling that the elastic modulus of the matrix is 1). It is noted that in definition (8), the effect of local variations of mass density (based on the local inclusion density) on the wave speed is not incorporated. If an SVE could hypothetically be formed only of the matrix phase, $c_M(\theta)$ would take the value of one for all angles.

5 Results

Results are presented showing the dependence of strength properties and maximum wave speed on the angle of loading for square and Voronoi SVE. Results are also presented showing convergence of material properties as a function of partition size for SVE generated using square and Voronoi partitioning.

5.1 Material Property Dependence on Angle of Loading.

In this section, results showing the dependence of SVE material properties on the angle of applied load are considered for square and Voronoi SVE. In the case of strength properties, either the tensile strength (\tilde{s}_n) or the shear strength (\tilde{s}_t) is divided by the threshold value of stress (σ^{TH}). The threshold stress is defined above as the maximum stress the matrix may reach at the matrix/inclusion boundary, in the direction normal to the inclusion, before failure is assumed. The variations of the normalized maximum wave speed c_M as a function of the wave direction θ are also considered.

To illustrate material property dependence on load angle, tensile strength (Figs. 3 and 4) and shear strength (Figs. 5 and 6) are plotted as a function of load angle.

Figure 3 shows tensile strength in square SVE, and can be compared with Fig. 4, showing the same result using Voronoi partitioned SVE. Overall, the mean value of tensile strength is greater in Voronoi SVE, and the range of values is narrower. A nearly sinusoidal pattern is seen in the Voronoi results, where minimum tensile strength occurs at $\theta = \pi/2$ with a period of $\pi/2$. The Voronoi results show this pattern significantly more strongly than the square SVE results.

Figure 5 shows shear strength in square SVE, and can be compared with Fig. 6, showing the same result using Voronoi partitioned SVE. As with tensile strength, the mean value of shear strength is greater in Voronoi SVE, and the range of values is slightly narrower at most load angles. Again, a sinusoidal pattern is clearly evident in the Voronoi results, and only mildly suggested in the square SVE results. In the case of shear strength, the local maximum occurs at $\theta = \pi/2$ such that the normal and shear strength functions exhibit a phase shift of $\pi/4$, when Voronoi results are compared.

To consider additional material properties, as well as additional SVE sizes, results are presented in Figs. 7–12. In these figures,

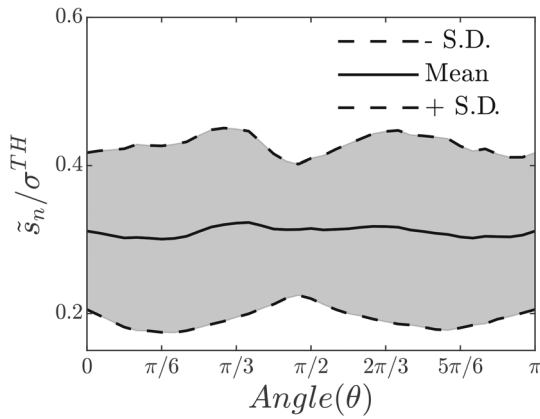


Fig. 3 Normalized tensile strength as a function of load angle θ for square SVE size $\delta = 1/8$

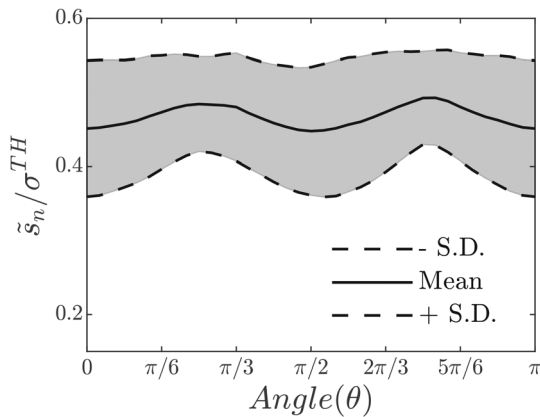


Fig. 4 Normalized tensile strength as a function of load angle θ for Voronoi SVE size $\delta = 1/8$

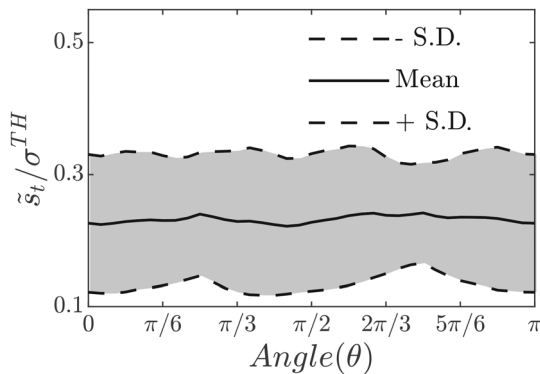


Fig. 5 Normalized shear strength as a function of load angle θ for square SVE size $\delta = 1/8$

mean material property values are given as a function of load angle for different sized SVE.

Figures 7 and 8 show tensile strength results for square and Voronoi SVE, respectively. In both Voronoi and square SVE, size of the SVE is inversely related to strength, both tensile and shear, as expected. Larger SVEs have a higher probability of containing weaker regions, which lower their strength value. The difference in SVE strength caused by the variation of SVE size is less pronounced for Voronoi SVE. The sinusoidal quality of the variation in mean tensile strength is consistent for Voronoi SVE across all SVE sizes δ . For example, all sizes of SVE display local minima

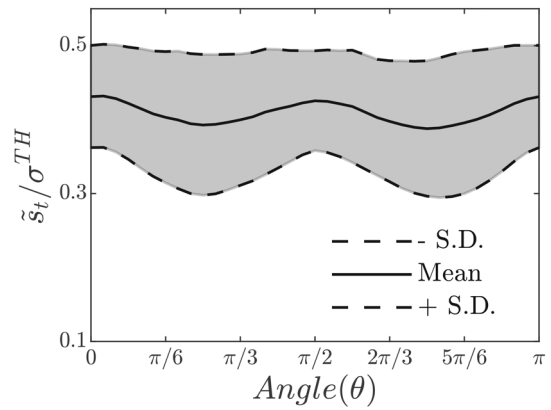


Fig. 6 Normalized shear strength as a function of load angle θ for Voronoi SVE size $\delta = 1/8$

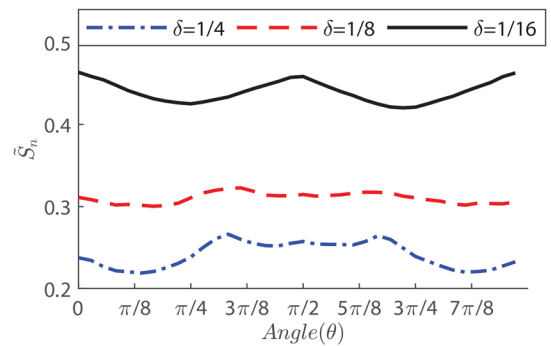


Fig. 7 Mean tensile strength as a function of load angle θ for square SVE. Strength is averaged over all SVE for a given SVE size $\delta = 1/4$, $\delta = 1/8$, and $\delta = 1/16$.

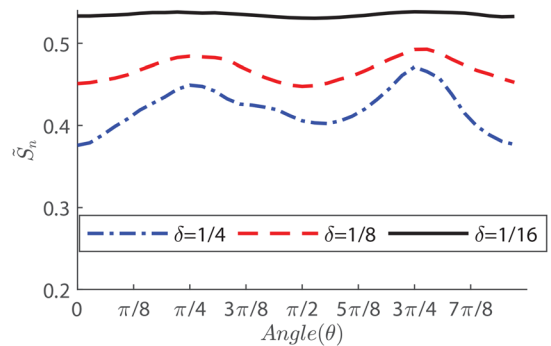


Fig. 8 Mean tensile strength as a function of load angle θ for Voronoi SVE. Strength is averaged over all SVE for a given SVE size $\delta = 1/4$, $\delta = 1/8$, and $\delta = 1/16$.

in tensile strength at approximately $\pi/2$ (Fig. 8). As δ increases, the amplitude of these curves is also seen to increase in the Voronoi case. For square SVE (Fig. 7), a sinusoidal pattern is only clearly observed at the smallest SVE size ($\delta = 1/16$), where, in contrast to the Voronoi case, a local maximum occurs at $\theta = \pi/2$.

Figures 9 and 10 show shear strength results for square and Voronoi SVE, respectively. These results are consistent with the tensile strength case, in that SVE size is inversely related to strength, variation in strength is less pronounced in Voronoi SVE, and sinusoidal variation is not clearly present in square SVE at large SVE sizes. Sinusoidal variation is observed in Voronoi SVE at all SVE sizes, with amplitude decreasing as SVE size decreases (such that the variation in $\delta = 1/16$ SVE is not easily visualized at the scale shown in Fig. 10). Comparing Figs. 8 and 10, Voronoi

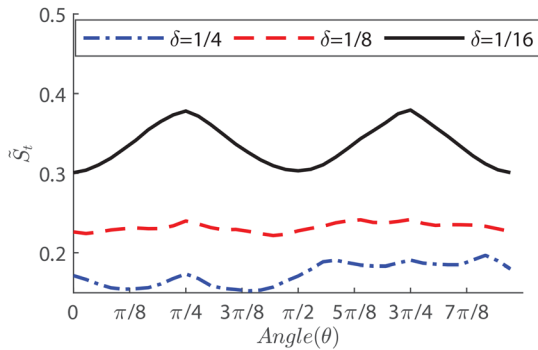


Fig. 9 Mean shear strength as a function of load angle θ for square SVE. Strength is averaged over all SVE for a given SVE size $\delta = 1/4$, $\delta = 1/8$, and $\delta = 1/16$.

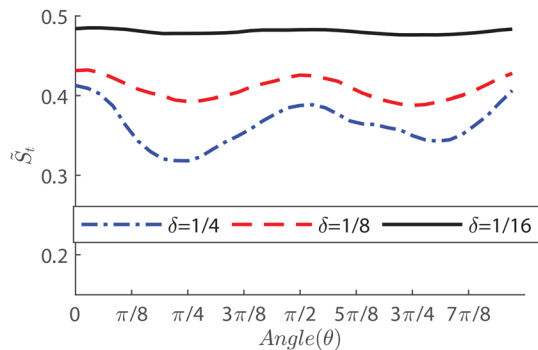


Fig. 10 Mean shear strength as a function of load angle θ for Voronoi SVE. Strength is averaged over all SVE for a given SVE size $\delta = 1/4$, $\delta = 1/8$, and $\delta = 1/16$.

tensile and shear strength functions suggest a phase shift of $\theta = \pi/2$. Comparing Figs. 7 and 9, a phase-shifted relationship is only evident in square SVE results at the smallest SVE size $\delta = 1/16$. Interestingly, the square (at $\delta = 1/16$) and Voronoi results are out of phase with a shift of $\theta = \pi/2$. This result is seen for tensile strength (Figs. 7 and 8) and shear strength (Figs. 9 and 10).

Figures 11 and 12 show maximum wave speed results for square and Voronoi SVE, respectively. In all cases, for all sizes δ and both square and Voronoi SVE, a clear sinusoidal pattern is observed, with maxima occurring at $\theta = \pi/2$, and with a period of $\pi/2$. For square SVE, the amplitude of the functions increases as the size δ decreases (i.e., the SVE are more anisotropic at smaller SVE sizes). For Voronoi SVE, the difference in amplitude between SVE of different sizes is much less pronounced.

Overall, these results show that the material property anisotropy obtained in an SVE analysis often corresponds to the angle of loading applied. In other words, anisotropy may not be a true property of the material, but rather an artifact of the choice of modeling (partitioning type and size, as well as the choice of boundary conditions).

Considering the applied loading (see Fig. 2), where the SVE has square boundaries (or in the case of the large size Voronoi SVE, relatively square boundaries), loading is aligned with SVE geometry at the angles $\theta = 0, \pi/2$, and π . Only in the small size Voronoi SVE do the SVEs display isotropy in the mean, or independence between the material strength properties recovered, and the applied angle of loading when the results of the SVEs are ensemble averaged. At a small length scale, the Voronoi SVEs are not square, but rather polygonal configurations such as the one pictured in Fig. 2. In these SVEs, the boundaries are nearly randomly aligned with respect to the angle of loading.

5.2 Convergence of Material Properties. In the results presented in this section, two measures are obtained for an

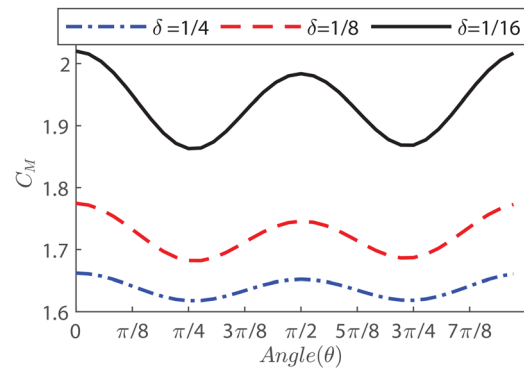


Fig. 11 Mean maximum wave speed as a function of load angle θ for square SVE. Strength is averaged over all SVE for a given SVE size $\delta = 1/4$, $\delta = 1/8$, and $\delta = 1/16$.

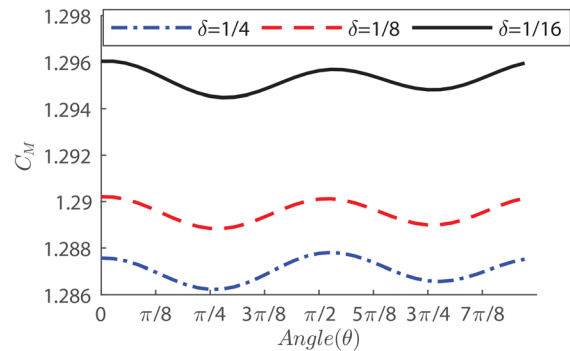


Fig. 12 Mean maximum wave speed as a function of load angle θ for Voronoi SVE. Strength is averaged over all SVE for a given SVE size $\delta = 1/4$, $\delta = 1/8$, and $\delta = 1/16$.

angle-dependent property homogenized at the SVE level. First, we consider the mean of a given property over all angles of applied loading. Specifically, \bar{S}_n is the mean value of the angle-dependent SVE strength $\tilde{s}_n(\theta)$ over angle θ ; that is $\bar{S}_n = \text{mean}_{\theta \in [0, \pi]} \tilde{s}_n(\theta)$. Similarly, $\bar{S}_t = \text{mean}_{\theta \in [0, \pi]} \tilde{s}_t(\theta)$ and $C_M = \text{mean}_{\theta \in [0, \pi]} C_M(\theta)$. These mean values are used to study the variation of the homogenized property for all the SVEs of one size, and across groups of SVEs with different sizes. They are, however, not suitable for studying the anisotropy of the homogenized properties. For this purpose for each SVE, we consider the standard deviation of the homogenized property. That is, we define $\sigma_{\tilde{s}_n} = \text{s.dev}_{\theta \in [0, \pi]} \tilde{s}_n(\theta)$, $\sigma_{\tilde{s}_t} = \text{s.dev}_{\theta \in [0, \pi]} \tilde{s}_t(\theta)$, and $\sigma_{C_M} = \text{s.dev}_{\theta \in [0, \pi]} C_M(\theta)$. Clearly, the higher the variation of a given angle-dependent field in an SVE over $\theta \in [0, \pi]$, the more anisotropic is that homogenized field for the given SVE.

Figures 13–15 show the convergence of material mean tensile strength \bar{S}_n , mean shear strength \bar{S}_t , and mean maximum wave speed C_M , respectively, as a function of SVE size for square and Voronoi partitioned SVE. In each case, the mean material property is plotted within an envelope showing range of the minimum and maximum values recovered for SVE of a given size.

Generally, convergence of mean, minimum, and maximum values is observed with increasing SVE size. This is expected, as larger SVE sizes approach the size of an RVE. Material strength (Figs. 13 and 14) tends to decrease with increasing SVE size. This is also expected, as larger SVEs have a higher likelihood of containing regions with large stress concentration, and therefore lower strength. This is the well-known *size-effect* [22,23] in which the mean and variation of fracture strength decrease as the size of a sampled domain increases. It is noted that for tensile strength (Fig. 13), the maximum SVE size studied in this analysis, $\delta = 1/4$, is not sufficient to capture convergence to mean values,

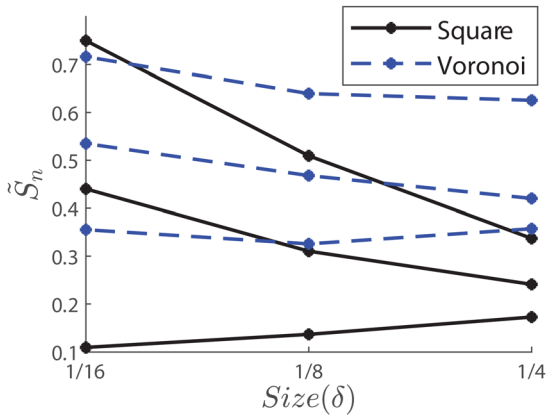


Fig. 13 Tensile strength as a function of SVE size δ for square and Voronoi SVE. Triple lines indicate minimum, mean, and maximum property values recovered from population of SVE with given size.

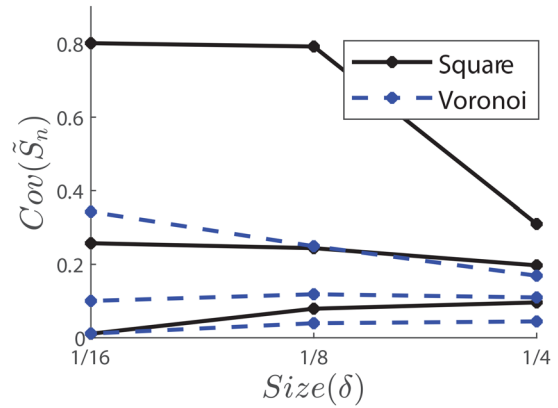


Fig. 16 Coefficient of variation of tensile strength as a function of SVE size for square and Voronoi SVE. The three lines represent the minimum, mean, and maximum of this anisotropy index across all SVEs of a given size.

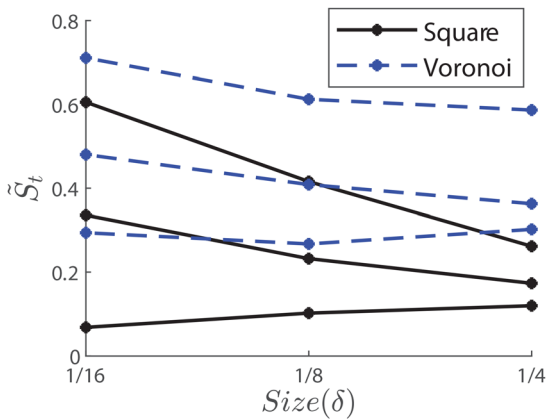


Fig. 14 Shear strength as a function of SVE size δ for square and Voronoi SVE. Triple lines indicate minimum, mean, and maximum property values recovered from population of SVE with given size.

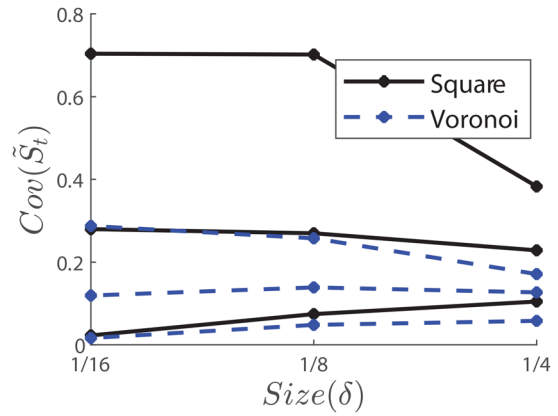


Fig. 17 Coefficient of variation of shear strength as a function of SVE size for square and Voronoi SVE. The three lines represent the minimum, mean, and maximum of this anisotropy index across all SVEs of a given size.

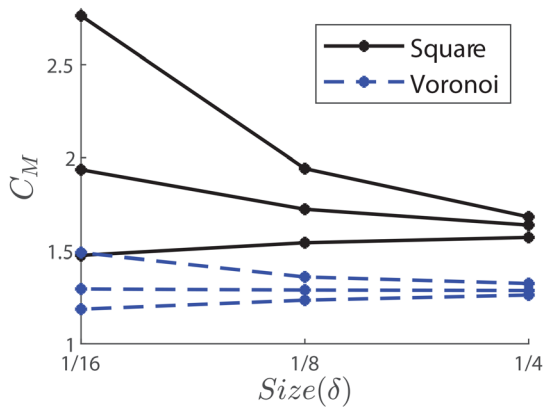


Fig. 15 Maximum wave speed as a function of SVE size δ for square and Voronoi SVE. Triple lines indicate minimum, mean, and maximum property values recovered from population of SVE with given size.

particularly for Voronoi SVE. In the case of larger SVE sizes, there are few number of SVE partitioning a given RVE, so statics are less accurate at larger SVE sizes. The maximum wave speed results show relatively strong convergence with increasing SVE size, compared to strength results.

Several interesting differences are observed between the two SVE types. For fracture strengths, square SVEs have a lower mean value for all the SVE sizes considered. Unlike Voronoi SVEs, the boundary of square SVEs can cut through the inclusions. The application of the SVE loads on square boundaries can cause severe stress concentrations at these sites, explaining the overall smaller strength of square SVEs. Moreover, we observe that both the mean and the range of the fracture strength decrease faster for square SVEs. This may appear to better model the size effect of this composite. In addition, in Refs. [24–27] and other similar studies, it is shown that fragmentation and fracture response of materials is more accurately modeled where fracture strength is variable, modeled as a random field. However, this stronger size effect is artificial, and is mainly caused by severe nonphysical stress concentration points on the boundary of square SVEs.

Next, we investigate the trend at which the anisotropy of a homogenized material property decreases versus the SVE size. The anisotropy of the homogenized properties of square and Voronoi SVEs is compared in Figs. 16–18. Similar to Figs. 13–15, the three lines for each data set correspond to the minimum, mean, and maximum of the anisotropy index across all the SVEs of a given size. That is for a given SVE size, the maximum and minimum values correspond to the most and least anisotropic sampled SVEs, whereas the mean values represent the overall anisotropy of the sampled property for that SVE size. From the decrease of

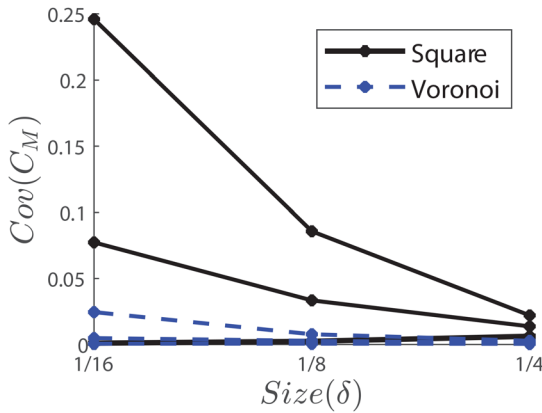


Fig. 18 Coefficient of variation of maximum wave speed as a function of SVE size for square and Voronoi SVE. The three lines represent the minimum, mean, and maximum of this anisotropy index across all SVEs of a given size.

the mean values in Figs. 16 and 17, we observe that the homogenized normal and shear strengths become more isotropic as higher SVE sizes are considered. Even the most anisotropic sampled SVEs tend to become more isotropic, since the maximum values also decrease versus the SVE size. Moreover, the homogenized strengths by Voronoi SVEs are less anisotropic than those from square SVEs. Finally, two main differences between elastic and fracture properties are observed. First, the maximum wave speed is almost isotropic for all Voronoi SVE sizes considered in Fig. 18. Second, even for square SVEs that exhibit a higher anisotropy, SVEs of size $\delta = 1/4$ are almost isotropic. In short, homogenized fracture properties are more anisotropic than the elastic properties, represented by c_M .

6 Conclusions

Results of this work highlight the utility of SVE homogenization methods based on Voronoi cell partitioning. Both elastic wave properties and strength properties are shown to converge more rapidly with increasing SVE size when Voronoi partitioning is used. This suggests that wide scatter in recovered material properties may often be due to stress concentrations on the boundaries of the SVE when inclusions intersect these partition boundaries. Eliminating this type of stress concentration gives a more accurate representation of the true variability of recovered properties due to geometric variation in material microstructure.

In addition to eliminating spurious stress concentrations on SVE boundaries, the geometry of Voronoi partitioning holds another advantage. The relatively random orientation of Voronoi SVE boundaries, particularly at small SVE sizes, decreases the angular dependency due to the chosen orientation of loading. SVE properties (unlike RVE properties) are by definition nonunique; therefore SVE data will reflect a dependency on the boundary conditions chosen in the analysis. However, partitioning with boundaries that are essentially randomly aligned with respect to loading directions is shown to decrease this dependency when results are ensemble averaged.

In future work, Voronoi partitioning will be used to model materials that have anisotropy due to material morphology. Voronoi partitioning is expected to be a more accurate means of capturing the true local behavior and variability in an anisotropic material. Improvements to this modeling technique will be considered, where SVE geometry is more randomly aligned, particularly at larger SVE sizes. The goal is to reduce the variability in recovered properties due to spurious effects (stress concentrations on the SVE boundary, alignment of SVE geometry with direction of applied load) so as to capture the authentic local variability of local material properties due to the morphology of the

microstructure. This true local variability contributes greatly to the initiation and propagation of cracks in brittle materials. The probabilistic local characterization of materials that are isotropic or anisotropic in bulk will be used to increase accuracy in simulating brittle fracture.

Funding Data

- U.S. National Science Foundation (NSF), CMMI—Mechanics of Materials and Structures (MoMS) program (Grant No. 1538332; Funder ID: 10.13039/501100008982).
- Supplemental funding from this award through a Research Opportunity Award (ROA) also supported research at the University of St. Thomas (Funder ID: 10.13039/100009768).

References

- [1] Hazanov, S., and Huet, C., 1994, "Order Relationships for Boundary Conditions Effect in Heterogeneous Bodies Smaller Than the Representative Volume," *J. Mech. Phys. Solids*, **42**(12), pp. 1995–2011.
- [2] Huet, C., 1990, "Application of Variational Concepts to Size Effects in Elastic Heterogeneous Bodies," *J. Mech. Phys. Solids*, **38**(6), pp. 813–841.
- [3] Ostoja-Starzewski, M., 2006, "Material Spatial Randomness: From Statistical to Representative Volume Element," *Probab. Eng. Mech.*, **21**(2), pp. 112–132.
- [4] Ostoja-Starzewski, M., 1998, "Random Field Models of Heterogeneous Materials," *Int. J. Solids Struct.*, **35**(19), pp. 2429–2455.
- [5] Gitman, I. M., Askes, H., and Sluys, L. J., 2007, "Representative Volume: Existence and Size Determination," *Eng. Fract. Mech.*, **74**(16), pp. 2518–2534.
- [6] Kanit, T., Forest, S., Galliet, L., Mounoury, V., and Jeulin, D., 2003, "Determination of the Size of the Representative Volume Element for Random Composites: Statistical and Numerical Approach," *Int. J. Solids Struct.*, **40**(13–14), pp. 3647–3679.
- [7] Baxter, S., and Graham, L., 2000, "Characterization of Random Composites Using Moving-Window Technique," *J. Eng. Mech.*, **126**(4), pp. 389–397.
- [8] Graham, L., and Baxter, S., 2001, "Simulation of Local Material Properties Based on Moving-Window Gmc," *Probab. Eng. Mech.*, **16**(4), pp. 295–305.
- [9] Graham-Brady, L., Siragy, E., and Baxter, S., 2003, "Analysis of Heterogeneous Composites Based on Moving-Window Techniques," *J. Eng. Mech.*, **129**(9), pp. 1054–1064.
- [10] Acton, K., and Graham-Brady, L., 2009, "Meso-Scale Modeling of Plasticity in Composites," *Comput. Methods Appl. Mech. Eng.*, **198**(9–12), pp. 920–932.
- [11] Weibull, W., 1951, "A Statistical Distribution Function of Wide Applicability," *ASME J. Appl. Mech.*, **18**(3), pp. 293–297.
- [12] Abedi, R., Omid, O., and Clarke, P., 2016, "Numerical Simulation of Rock Dynamic Fracturing and Failure Including Microscale Material Randomness," *50th U.S. Rock Mechanics/Geomechanics Symposium*, Houston, TX, June 26–29, Paper No. ARMA 16-0531.
- [13] Abedi, R., Haber, R. B., and Clarke, P. L., 2017, "Effect of Random Defects on Dynamic Fracture in Quasi-Brittle Materials," *Int. J. Fract.*, **208**(1–2), pp. 241–268.
- [14] Koyama, T., and Jing, L., 2007, "Effects of Model Scale and Particle Size on Micro-Mechanical Properties and Failure Processes of Rocks—A Particle Mechanics Approach," *Eng. Anal. Boundary Elem.*, **31**(5), pp. 458–472.
- [15] Acton, K., Baxter, S., Bahmani, B., Clarke, P., and Abedi, R., 2017, "Mesoscale Models Characterizing Material Property Fields Used as a Basis for Predicting Fracture Patterns in Quasi-Brittle Materials," *ASME Paper No. IMECE2017-71500*.
- [16] Clarke, P., Abedi, R., Bahmani, B., Acton, K., and Baxter, S., 2017, "Effect of the Spatial Inhomogeneity of Fracture Strength on Fracture Pattern for Quasi-Brittle Materials," *ASME Paper No. IMECE2017-71515*.
- [17] Salmi, M., Auslender, F., Bornert, M., and Fogli, M., 2012, "Apparent and Effective Mechanical Properties of Linear Matrix-Inclusion Random Composites: Improved Bounds for the Effective Behavior," *Int. J. Solids Struct.*, **49**(10), pp. 1195–1211.
- [18] Acton, K. A., and Baxter, S. C., 2018, "Characterization of Random Composite Properties Based on Statistical Volume Element Partitioning," *J. Eng. Mech.*, **144**(2), p. 04017168.
- [19] Acton, K. A., Baxter, S. C., Bahmani, B., Clarke, P. L., and Abedi, R., 2018, "Voronoi Tessellation Based Statistical Volume Element Characterization for Use in Fracture Modeling," *Comput. Methods Appl. Mech. Eng.*, **336**, pp. 135–155.
- [20] Nguyen, V. P., Lloberas-Valls, O., Stroeve, M., and Sluys, L. J., 2011, "Homogenization-Based Multiscale Crack Modelling: From Micro-Diffusive Damage to Macro-Cracks," *Comput. Methods Appl. Mech. Eng.*, **200**(9–12), pp. 1220–1236.
- [21] Daphalapurkar, N., Ramesh, K., Graham-Brady, L., and Molinari, J., 2011, "Predicting Variability in the Dynamic Failure Strength of Brittle Materials Considering Pre-Existing Flaws," *J. Mech. Phys. Solids*, **59**(2), pp. 297–319.
- [22] Bazant, Z. P., and Planas, J., 1997, *Fracture and Size Effect in Concrete and Other Quasibrittle Materials*, Vol. 16, CRC Press, New York.

- [23] Bazant, Z. P., and Le, J.-L., 2017, *Probabilistic Mechanics of Quasibrittle Structures: Strength, Lifetime, and Size Effect*, Cambridge University Press, New York.
- [24] Zhou, F., and Molinari, J., 2004, "Stochastic Fracture of Ceramics Under Dynamic Tensile Loading," *Int. J. Solids Struct.*, **41**(22–23), pp. 6573–6596.
- [25] Schicker, J., and Pfuff, M., 2006, "Statistical Modelling of Fracture in Quasi-Brittle Materials," *Adv. Eng. Mater.*, **8**(5), pp. 406–410.
- [26] Levy, S., and Molinari, J., 2010, "Dynamic Fragmentation of Ceramics, Signature of Defects and Scaling of Fragment Sizes," *J. Mech. Phys. Solids*, **58**(1), pp. 12–26.
- [27] Bahmani, B., Yang, M., Nagarajan, A., Clarke, P. L., Soghrati, S., and Abedi, R., 2019, "Automated Homogenization-Based Fracture Analysis: Effects of SVE Size and Boundary Condition," *Comput. Methods Appl. Mech. Eng.*, **345**, pp. 701–727.